Characterization of the MIRO-independent mitochondrial association activity of TRAK proteins

Lili Mitchell, Kathryn E. Reda, Hijab Fatima, Claudia E. Vasquez, and Omar A. Quintero-Carmona

Department of Biology, University of Richmond, VA 23173

Running head: MIRO-independent MOM association of TRAK

Corresponding author:

Omar A. Quintero-Carmona
Department of Biology
University of Richmond
138 UR Drive
Richmond, VA 23173
Office: (804)287-6892
Lab: (804) 289-1706
FAX (804) 289-8233
Email: oquinter@richmond.edu

Stats (words/characters)

Title page:	66/447
Abstract:	203/1308
Introduction:	693/4241
Results & Discussion:	2346/14210
Acknowledgements:	218/1111
Figure Legends:	590/3602
Supplemental Legends:	562/3427
Materials & Methods:	1244/7051

Abstract

Current models suggest that MIRO GTPases anchor cytoskeletal motors to the mitochondrial outer membrane (MOM). However, our previous findings indicate that the unconventional myosin, MYO19, interacts with MIRO weakly but that a MIRO-independent MOM-localizing domain interacts more tightly with the MOM. To test the model that MIRO proteins serve as weaker, initial recruiters of cytoskeletal motors to mitochondria, we examined interactions between TRAK proteins (microtubule motor-mitochondria adapter proteins) and the MOM via quantitative fluorescence microscopy and steady-state kinetic approaches. Using GFP-TRAK truncations expressed in MIRO1-2 double knockout mouse embryonic fibroblasts, we identified a MIRO-independent mitochondrial binding domain in the C-terminus of TRAK1 and TRAK2, sufficient for localization to the MOM--similar to what we observed for full length GFP-TRAK proteins. The MIRO-binding domains (MBD) of the TRAK proteins were only able to localize to mitochondria in the presence of ectopic expression of MIRO. Importantly, fluorescence recovery after photobleaching (FRAP) demonstrated that the steady-state kinetics of $TRAK^{MBD}$/MIRO2 interaction were faster-exchanging than for either full-length TRAK or the TRAK C-terminal MOM-binding domain expressed alone. These data support the model that MIRO supports weak associations of cytoskeletal motors to the MOM, while MIRO-independent binding contributes significantly to tighter association of such motors to the MOM.

Introduction

Mitochondria serve many biological roles. In addition to adenosine triphosphate (ATP) synthesis, mitochondria participate in intracellular calcium homeostasis, regulate reactive oxygen species, and are central to apoptotic activities (Wang and Youle, 2009). The proper positioning of mitochondria within cells is essential for these activities and for maintaining cellular health. Improper localization can contribute to abnormal mitochondrial functioning which may contribute to degenerative diseases, metabolic diseases, and cancer (Wallace, 1999). Mitochondria positioning defects are implicated in neuronal dysfunction linked to Alzheimer's and Parkinson's disease (DiMauro, 1999). The study of mitochondrial localization, network organization, and transport are therefore important in providing foundational understanding of biological function and well as for developing treatment options for many serious diseases.

Mitochondria are dynamic organelles which are constantly dividing, fusing, and moving throughout the cytosol (Fenton et al., 2020). Mitochondria localize to different regions of the cell through interactions with motor proteins like kinesin, dynein, and MYO19. Attachment of these motors to mitochondria enable movement across cytoskeletal networks of microtubules and actin filaments. Actin-based mitochondrial movement is facilitated by interactions with a mitochondria-associated unconventional myosin, MYO19 (Quintero et al., 2009), while microtubule based motility is regulated by kinesins (Smith et al., 2006) and dynein (Pilling et al., 2006; van Spronsen et al., 2013). Many recent reports have implicated the small rho-like GTPase, MIRO, as a receptor for motor proteins on the mitochondrial outer membrane (Glater et al., 2006; Guo et al., 2005; MacAskill et al., 2009; van Spronsen et al., 2013; Wang and Schwarz, 2009).

Microtubule motor protein interactions with MIRO on the MOM are thought to involve adaptors. Originally identified in *Drosophila*, TRAK proteins (also known as Milton) were thought to facilitate binding between MIRO proteins and microtubule-based motors (Stowers et al., 2002). Two mammalian TRAK proteins have been identified, TRAK1 and TRAK2, which share ~58% amino acid homology (Beck et al., 2002; Iyer et al., 2003). The study of MIRO in a mitochondrial context has historically centered around its role in anchoring TRAK and molecular motors to the MOM (Fransson et al., 2003; Fransson et al., 2006). Though the precise mechanisms of MIRO, TRAK, and motor protein interactions have not been well established, the N-terminal region of TRAK family proteins contain a kinesin-interacting domain (Smith et al., 2006) as well as coiled-coil regions that may facilitate homodimerization (Glater et al., 2006; Stowers et al., 2002). Additional N-terminal regions mediate interactions with dynein complexes (Fenton et al., 2021), and the TRAK proteins also contain a central, MIRO-binding domain region (MBD) consisting of approximately 220 amino acids (MacAskill et al., 2009). These findings have shaped the perception of MIRO as a required component of mitochondrial localization (Guo et al., 2005). However, there is evidence that TRAK may interact with mitochondria independently of its association with MIRO. Recent studies have shown that when TRAK is expressed in cells lacking endogenous MIRO, TRAK proteins still localize to mitochondria (Lopez-Domenech et al., 2018), suggesting alternative mechanisms for TRAK/MOM interaction and potentially a distinct role for MIRO in MOM/motor interactions beyond serving as an anchor.

In considering the mechanism of interaction between mitochondria and MYO19, Bocanegra and colleagues proposed a model where MIRO proteins serve in initial recruitment steps of MYO19 to mitochondria, and that a second, MIRO-independent mechanism facilitates

longer-term docking between the MOM and MYO19 (Bocanegra et al., 2019). The discovery of MIRO-independent TRAK binding to the MOM by Lopez-Domenech and colleagues led us to the hypothesis that MIRO proteins may also serve in a "recruitment" role for TRAK/MOM interactions, while MIRO-independent mechanisms have stronger associations with the MOM. We combined end-point quantitative microscopy approaches paired with fluorescence recovery after photobleaching (FRAP) analyses of dynamic behaviors to investigate properties of TRAK/MOM/MIRO interactions. We then used those observations to develop a more nuanced model for MIRO function as an initial recruiter of cytoskeletal motors and their adapters to the MOM. We were able to localize the MIRO-independent MOM binding domain to the C-terminus of both TRAK1 and TRAK2, and steady-state kinetic data lends further support to a model where MIRO proteins serve in the faster-dissociating, initial recruitment of proteins to the MOM, while MIRO-independent binding mediates slower-dissociating interactions with the mitochondria.

Results and Discussion

Ectopic MIRO2 expression enhances TRAK binding to mitochondria

HeLa cells were used to quantify the impact of increased MIRO expression on the association of GFP-TRAK constructs with mitochondria via mito-cyto ratio analysis. Transfection conditions were chosen so that levels of ectopic expression were limited. GFP-tagged versions of either TRAK showed enriched mitochondrial localization relative to cytosolic localization (MCR>1), and ectopic mchr-MIRO2 expression enhanced the localization of GFP-TRAK proteins to mitochondria (Figure 1A and 1C). Ectopic expression of mchr-MIRO2 also enhanced GFP-TRAK^{MBD} localization to mitochondria, with little evidence of mitochondrial localization of the TRAK^{MBD} constructs in the absence of ectopic mchr-MIRO2 (Figure 1B and 1D). HeLa cells endogenously express both MIRO1 and MIRO2 (Oeding et al., 2018), so it may be initially surprising that TRAK^{MBD} constructs did not localize strongly to mitochondria when expressed in the absence of exogenous mchr-MIRO2. As the interaction between TRAK^{MBD} and MIRO2 may be a potentially low-affinity interaction, these results suggest that the endogenous levels of MIRO expression in HeLa cells are such that GFP-TRAK^{MBD} binding is not readily detectable by our method.

As the full-length GFP-TRAK proteins displayed easily observable mitochondrial localization in the absence of ectopic MIRO expression (MCR ~2), and the MIRO-enhancement of TRAK^{MBD} localization was not as pronounced (MCR ~1.3), we surmised that the mitochondrial localization displayed by the full-length GFP-TRAK constructs was not solely due to TRAK-MIRO interactions. López-Doménech and colleagues recently generated mouse embryonic fibroblasts lacking MIRO1 or MIRO2 expression--MEF^{dko} cells. Although MIRO proteins are often described as the linkage between the MOM and TRAK proteins (and often

illustrated this way, Fenton et al., 2020; Kruppa and Buss, 2021; Panchal and Tiwari, 2021), when MEF^{dko} cells were characterized, TRAK proteins could be detected in mitochondria-enriched cellular fractions and GFP-TRAK proteins localized with mitochondrial markers, lending further support to the presence of a MIRO-independent MOM-binding domain in TRAKs (Lopez-Domenech et al., 2018).

To further investigate how the presence of MIRO proteins influenced TRAK localization to the MOM, we repeated MCR analysis for GFP-TRAK constructs in MEF^{dko} cells. In this cellular context, full-length GFP-TRAK constructs still display an MCR >1, and expression of mchr-MIRO2 increased the MCR for GFP-TRAK2 (Figure 2A). Expression of mchr-MIRO2 was required for mitochondrial localization of GFP-TRAK^{MBD} constructs (Figure 2B). To further characterize the prevalence of the observed phenotypes, population phenotype analysis was performed in MEF^{dko} cells expressing different combinations of GFP-TRAK and mchr-MIRO2 constructs. Ectopic expression of mchr-MIRO2 reduced the fraction of cells displaying a cytosolic GFP distribution in cells coexpressing GFP-TRAK1, GFP-TRAK2, or GFP-TRAK2^{MBD}, but not for GFP-TRAK1^{MBD} (Figure 2C). The differential impact of MIRO2 expression on GFP-TRAK1 versus GFP-TRAK2 constructs in both MCR and population analyses could indicate differences in affinity for MIRO2 between the two TRAK isoforms and potential differences in cellular roles between TRAK1 and TRAK2 as well as between MIRO1 and MIRO2 (Lopez-Domenech et al., 2018; van Spronsen et al., 2013). Taken together, these findings confirm a MIRO-independent mechanism of TRAK localization to the MOM, and that this interaction may be the dominant mechanism of interaction between TRAK and the MOM as it is sufficient for mitochondrial localization even in the absence of MIRO.

MIRO-independent mitochondrial localization is encoded by the C-terminus of TRAK proteins

To investigate which region of TRAK facilitates MIRO-independent binding, we generated GFP-TRAK truncations encoding for the N-terminal region before the MBD and the C-terminal region after the MBD for both TRAK1 and TRAK2 (Figure S3A). When expressed in MEF^{dko} cells, neither of the N-terminal TRAK constructs showed enhanced mitochondrial localization, while both C-terminal constructs did display an MCR >1 (Fig. 3A and 3B). Population phenotype analyses also revealed similar behavior--cells expressing the GFP-TRAK N-terminal construct displayed primarily cytosolic GFP fluorescence while cells expressing the C-terminal construct had a greater fraction of intermediate and mitochondrial GFP localization, further supporting the presence of a MIRO-independent MOM association domain encoded by the C-terminus of TRAK (Figure 3C).

We attempted to identify the minimal MOM association domain ($TRAK^{min\text{-}C}$) by using MemBrain3.1 (Feng et al., 2022), which was employed by Shneyer and colleagues in identifying the MIRO-independent MOM interacting domain found in MYO19 (Shneyer et al., 2016). The $TRAK^{min\text{-}C}$ sequences predicted by MemBrain were also predicted by AlphaFold (Jumper et al., 2021; Varadi et al., 2022) to contain alpha helical regions (Figure S1). However, neither GFP-$TRAK1^{min\text{-}C}$ nor GFP-$TRAK2^{min\text{-}C}$ constructs localized to mitochondria in MEF^{dko} cells, whether the GFP-tag was at the N-terminus of the truncation or the C-terminus of the truncation (data not shown). The predictive power of the informatic approaches were insufficient in this instance. The potential TRAK binding partners mediating this interaction have yet to be determined, and many potential candidates have been identified via proteomic analyses (Oughtred et al., 2021).

The differences in the FRAP kinetics of the TRAK domains responsible for mitochondrial binding indicate differences in association with the MOM

Fluorescence recovery after photobleaching (FRAP) was performed to determine the kinetic properties of TRAK/MOM interactions mediated through MIRO-dependent or MIRO-independent mechanisms. Full-length GFP-TRAK1 and GFP-TRAK $1^{C\text{-term}}$ expressed in MEF^{dko} cells had a slower rate of exchange compared to that of GFP-$TRAK1^{MBD}$ expressed in combination with mchr-MIRO2 (Fig. 4A), and similar results were observed with GFP-TRAK2 constructs (Fig. 4B). GFP-$TRAK^{MBD}$ constructs expressed in combination with mchr-MIRO2 had significantly faster $t_{1/2}$, compared to their corresponding full-length construct expressed in the absence of MIRO2 (Figure 4 and S2). GFP-$TRAK^{C\text{-term}}$ constructs displayed FRAP kinetics far more similar to the full-length construct, although their $t_{1/2}$ were not quite as large as those of the full-length constructs.

The differences in FRAP kinetics between the full-length and C-terminal constructs in combination parallel what was observed with end-point measures. The observed enhancements in mitochondrial localization (Figure 3) observed with the C-terminal constructs was less robust than what was seen with the full-length constructs, and it is possible that regions in the N-terminus insufficient for mitochondrial localization enhance the properties encoded by the C-terminus. Multimerization through coiled-coil domains found in the N-terminus (Glater et al., 2006; Stowers et al., 2002) would serve to increase the valence of MOM association domains in any one protein assembly, influencing its MOM interactions. To investigate this question, conducted FRAP analysis on GFP-TRAK constructs lacking the MIRO-binding domain (GFP-$TRAK^{\Delta MBD}$). The observed $t_{1/2}$ for these constructs were slower than the $t_{1/2}$ for the corresponding GFP-$TRAK^{C\text{-term}}$ construct and similar in order of magnitude to the $t_{1/2}$ observed

with the full-length constructs, supporting the hypothesis that N-terminal sequences are necessary for dissociation kinetics similar to that of the full-length protein even though they are insufficient to encode for MOM localization (Figure 4 and S2).

To establish frames of reference for other putative components of motor complexes on the MOM in a similar cellular context, we completed FRAP analyses for GFP-MIRO2, and for the regions of MYO19 capable of MIRO-dependent (GFP-MYO19^{MBD} expressed with mchr-MIRO2) and MIRO-independent (GFP-MYO19^{mem}) mitochondrial association in MEF^{dko} cells. As we had previously reported in HeLa cells (Bocanegra et al., 2019), the $t_{1/2}$ for GFP-MYO19^{mem} was larger than that of GFP-MYO19^{MBD}/mchr-MIRO2, indicating faster exchange for MIRO-mediated association. It is worth noting that the $t_{1/2}$ of the apparent GFP-MYO19^{MBD}/mchr-MIRO2 interaction was slower in MEF^{dko} cells than what was previously reported in HeLa cells. One possible explanation for this difference is the cellular context. HeLa cells express MIRO1 and MIRO2, and the sum of endogenous and exogenous binding sites for GFP-MYO19^{MBD} could result in increased opportunities for exchange and an apparent faster recovery of fluorescence. Additionally, the $t_{1/2}$ for GFP-MIRO2 was of similar magnitude to that of GFP-MYO19^{mem} and slower than any of the GFP-TRAK constructs containing MIRO-independent MOM binding ability (Figure S2), suggesting that the MIRO-independent mechanisms binding to the MOM may differ mechanistically between MYO19 and TRAK.

These analyses suggest that GFP-TRAK^{cterm} interactions with the MOM have a stronger association than the GFP-TRAK^{MBD} interaction with mchr-MIRO2. As the kinetics of full-length GFP-TRAK are also significantly slower than those between GFP-TRAK^{MBD} and mchr-MIRO2, these data suggest that the TRAK^{MBD} interaction with MIRO facilitates an initial, weaker recruitment of the mitochondria while TRAK^{cterm} is partially responsible for slower turnover and

stronger interactions between TRAK and the MOM. As we observed with the MCR analysis, the quantitative difference between the full-length GFP-TRAK construct and the GFP-TRAK^{MBD}/mchr-MIRO2 interaction is not recapitulated to the same magnitude by the GFP-TRAK^{cterm} construct. This likely indicates that while the N-terminal TRAK sequences are insufficient for MIRO-independent interactions with the MOM, they may still play an important role in enhancing MOM association. Specifically, just as multimerization of motor proteins influences the time-fraction that the proteins are associated with their cytoskeletal filament (Howard, 2001), dimerization of TRAK through the N-terminal coiled-coil domains would enhance the likelihood of a protein assembly binding to the MOM as the multimer contains more binding sites than the monomer.

Kinetic considerations influence our understanding of MIRO function in the recruitment of cytoskeletal motors to mitochondria

Current models suggest that MIRO "anchors" TRAK proteins to the mitochondrial membrane (Kruppa and Buss, 2021). This interpretation is likely a consequence of experimental design--many of the previous experimental examinations of MIRO/TRAK interactions were carried out as end-point assays. Cells were made to express (or not express) a set of proteins under particular conditions, and then "fixed in time" for analysis. These analyses included assaying for binding via immunoprecipitation, or for co-occurrence via qualitative fluorescence microscopy. These experimental approaches do not address a key component required for full understanding of biologically relevant protein-protein interactions. Additionally, qualitative image analysis approaches make it more difficult to validate and compare results between experimental conditions (Wait et al., 2020).

Kinetic descriptors are crucial to informing a more complete biological understanding (Pollard and De La Cruz, 2013), and we believe this to be the first reported kinetic analysis of TRAK/MIRO interactions. In taking a quantitative and kinetic approach to our experimental design, we were able to identify relevant differences in the biochemical behavior of specific segments of the TRAK protein sequence with respect to MOM association. Population and MCR analyses in MEF^{dko} cells lacking MIRO expression enabled us to determine that TRAK was capable of MIRO-independent mitochondrial localization (Figure 2) and that the C-terminus of TRAK encoded for this property (Figure 3). Quantitative fixed-cell endpoint assays supported the idea that this interaction likely has different properties than that of the $TRAK^{MBD}$/MIRO interaction, and it is worth noting that the $TRAK^{C\text{-}term}$ does not overlap with the sequences involved in dynein or kinesin interactions (Fenton et al., 2021). We were able to demonstrate differences in binding kinetics between MIRO-dependent and MIRO-independent interactions with the MOM only by employing experimental approaches that allowed quantification of dynamic molecular processes (Figure 4 and Figure S2).

A revised model for the role of MIRO in motor protein/mitochondria interactions

The application of kinetic approaches led us to a model of MIRO function where the role of MIRO is as the initial acceptor of motor proteins to the mitochondrial outer membrane, while other mechanisms are responsible for longer-lived attachments (Figure 5). Our observations with TRAK proteins parallel what we had previously reported for MYO19, where kinetic analysis of MYO19/MIRO interactions first revealed that MIRO may provide fast-exchanging binding sites on the MOM for proteins that also contained a second, slower exchanging MOM association domain (Bocanegra et al., 2019). In this way, MIRO provides an initial mechanism of

recruitment of cytoskeletal motors and their adapters to the MOM, potentially increasing their local concentration. This would increase the rate of formation for MIRO-independent interactions with the MOM which might be tighter binding, but might also be lower probability events.

This idea is supported by the observations by Oeding and colleagues as well as Lopez-Domenech and colleagues (Lopez-Domenech et al., 2018; Oeding et al., 2018). Both groups observed that in cells lacking MIRO proteins, MYO19 levels decreased significantly. Their data also supported the interpretation that without MIRO proteins to assist in the insertion of MYO19 with the MOM, MYO19 remains cytosolic: accessible to ubiquitination and proteasome-mediated degradation.

It is curious that mitochondria-associated TRAK protein persist in the absence of MIRO expression even though a similar pattern for the kinetics of MIRO-dependent (faster) versus MIRO-independent (slower) MOM association was observed. This could be explained by the difference in $t_{1/2}$ between the MIRO-independent interactions for TRAK proteins and MYO19. The faster $t_{1/2}$ for MIRO-independent TRAK interactions may still happen at rates sufficiently quick to generate a population of mitochondria-bound TRAK protected from proteolysis, while the MIRO-independent MOM binding for MYO19 might be so rare that nearly all cellular MYO19 is susceptible to proteasome activity in the absence of MIRO.

If MIRO proteins primarily regulate the initial attachment to the MOM and are less involved in long-term association, then the role of the nucleotide state dependence of MIRO on the availability of the MOM for motor attachment may need to be reevaluated. The current model of MIRO activity is that MIRO is active and bound to cytoskeletal motors in one nucleotide state, while, favoring the dissociation of motors in a different nucleotide state

(Fransson et al., 2003; MacAskill et al., 2009). Our data indicate that the nucleotide state dependence of MIRO is not simply turning the molecular switch from “motors on” or “motors off,” where a mitochondrial network having only GDP-MIRO would be devoid of motors as they would have dissociated. Instead our data support a model where active MIRO simply facilitates recruitment. As MIRO interactions with motors are not the exclusive mechanism of mitochondrial interaction, other mechanisms, such as regulated degradation, would be responsible for controlling motor protein persistence on the MOM. Future investigations could involve kinetic assays to determine the role of ubiquitin-mediated proteolysis pathways on MOM-associated motor protein levels, and if the lifetime of TRAK adaptors and motor proteins on the MOM is sensitive to particular cellular conditions, such as glucose starvation, inner mitochondrial membrane potential, or cell-cycle state. As our experiments reveal that the homeostatic mechanisms regulating motor protein adaptor attachment to the mitochondria are partially independent of MIRO, developing a more complete understanding of the additional processes regulating motor protein adaptor attachment will be crucial to understanding the dynamics of mitochondria as an essential organelle in cellular physiology.

Acknowledgements

We would like to thank University of Richmond School of Arts and Science for funding and supporting undergraduate-driven research in the midst of the COVID pandemic. Christie Lacy's efforts as Director of Imaging and Microscopy, supporting our work while maintain the Imaging Core Facility were essential for the success of this project—we could not make these discoveries without the Core Facility and its Director. We would also like to thank Dr. Andrew Moore (HHMI-Janelia), Dr. Rebecca Adikes (Siena College), and Dr. Teng-Leong Chew (HHMI-Janelia) for giving their time to run out Zoom Image Analysis Bootcamp, introducing "the TRAK team" to the beauty of image quantitation. It opened the door for a bunch of naïve undergrads to be scientists even when we could not be in the lab.

Hypotheses and experiments in this study were conceived by OAQ and LM. Experiments were performed by LM, and OAQ. Data analysis was completed by LM, KR, HF, CV, and OAQ. Manuscript preparation was completed by LM with assistance from KR and OAQ. This work was funded through University of Richmond Arts & Sciences Summer Fellowships to LM, KR, and CV. HF and OAQ were funded by NIH R15 GM119077 to OAQ. A special thank you to Drs. Josef Kittler and Guillermo López-Doménech (University College London) for the MEF^{dko} cells.

Figures

Figure 1: Quantitative image analysis of TRAK1 & TRAK2 localization shows that ectopic expression of mchr-MIRO2 enhances TRAK-binding to mitochondria in HeLa cells. (A) Full length GFP-TRAK1 or GFP-TRAK2 localized more strongly to mitochondria than to the cytoplasm as indicated by a MCR >1, and enrichment was enhanced by ectopic expression mchr-MIRO2 (*$p<0.05$, t-test, $n \geq 86$ cells per condition). (B) GFP-TRAK^{MBD} constructs did not show mitochondrial enrichment except when expressed in combination with mchr-MIRO2 expression (*$p<0.05$, t-test, $n \geq 99$ cells per condition). Panels (C) and (D) show representative images of the most common patterns observed in cells expressing GFP-TRAK2 and mchr-MIRO2 constructs. Scale bar, 10 μm.

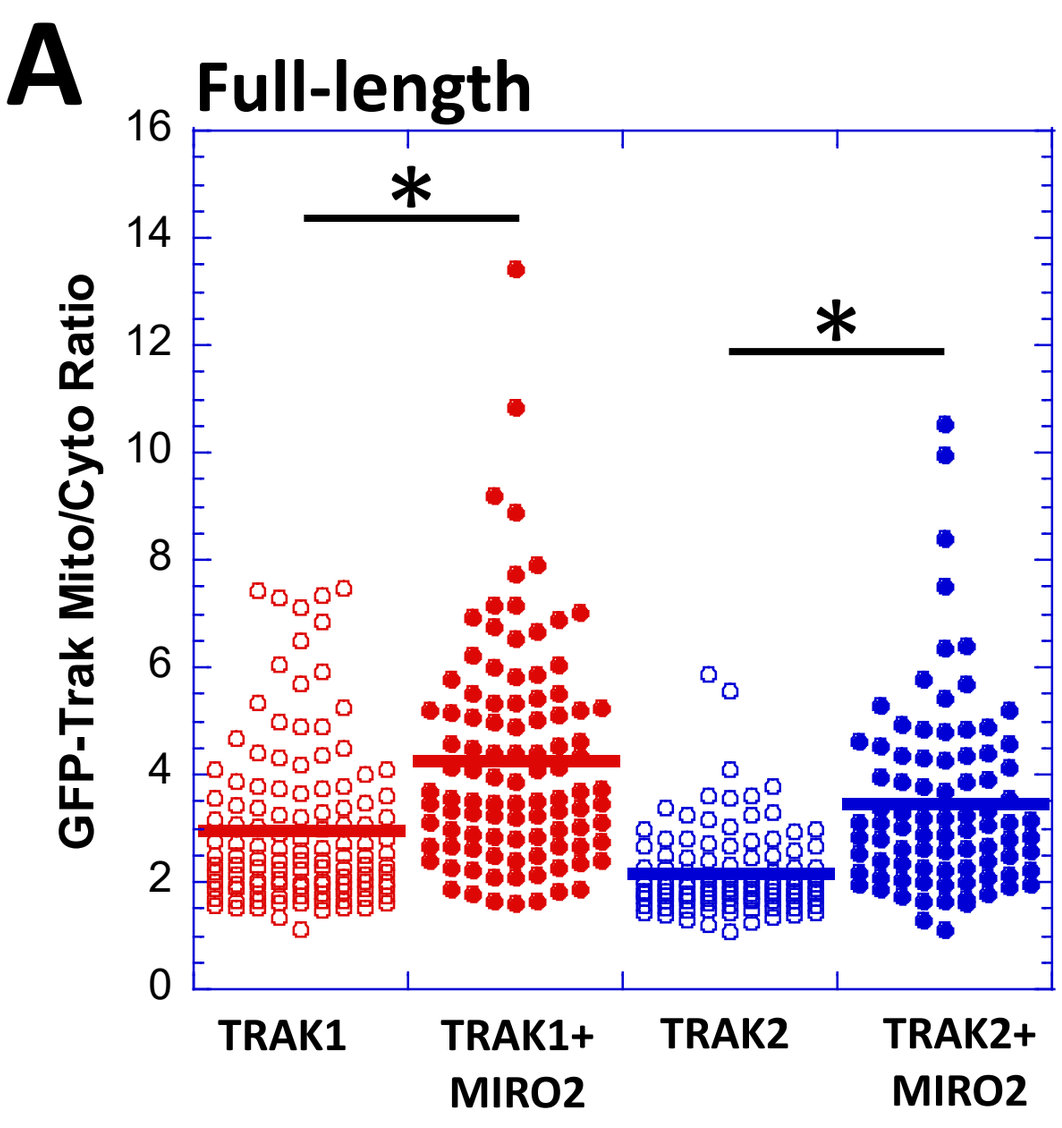
A
Full-length
GFP-Trak Mito/Cyto Ratio
16
14
12
10
8
6
4
2
0
*
*
TRAK1
TRAK1+ MIRO2
TRAK2
TRAK2+ MIRO2

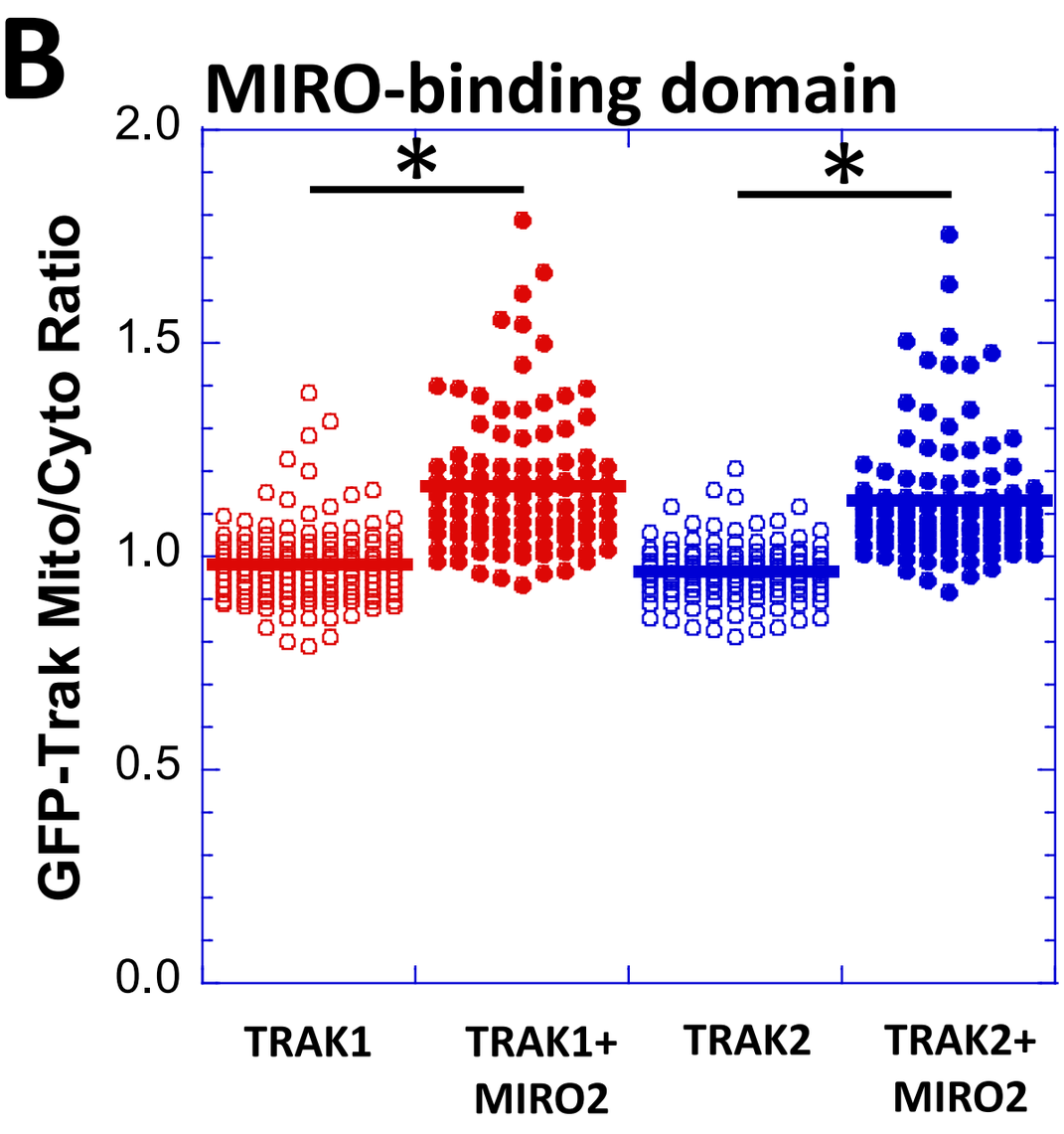
B
MIRO-binding domain
GFP-Trak Mito/Cyto Ratio
2.0
1.5
1.0
0.5
0.0
*
*
TRAK1
TRAK1+ MIRO2
TRAK2
TRAK2+ MIRO2

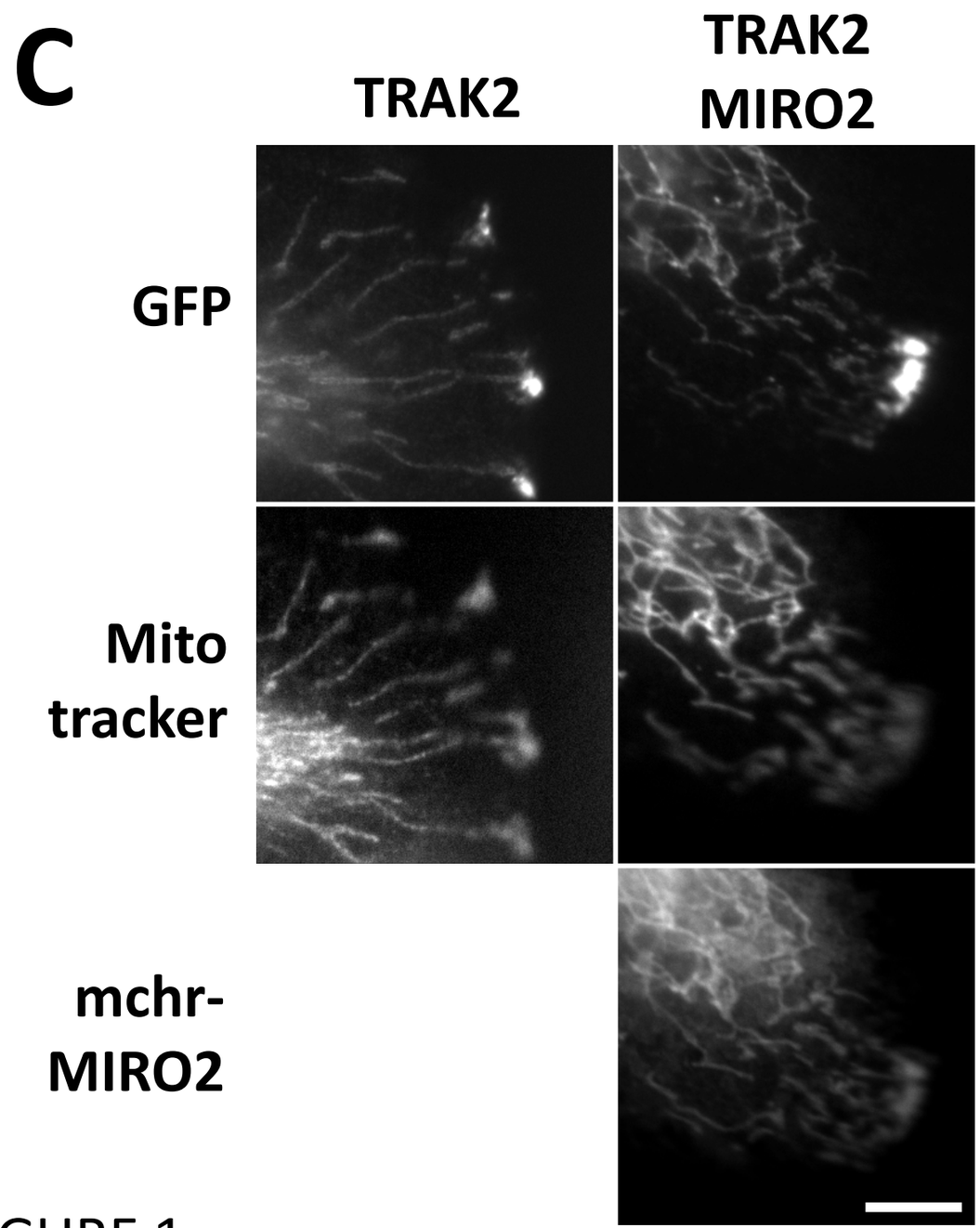
C
TRAK2
TRAK2 MIRO2
GFP
Mito tracker
mchr-MIRO2

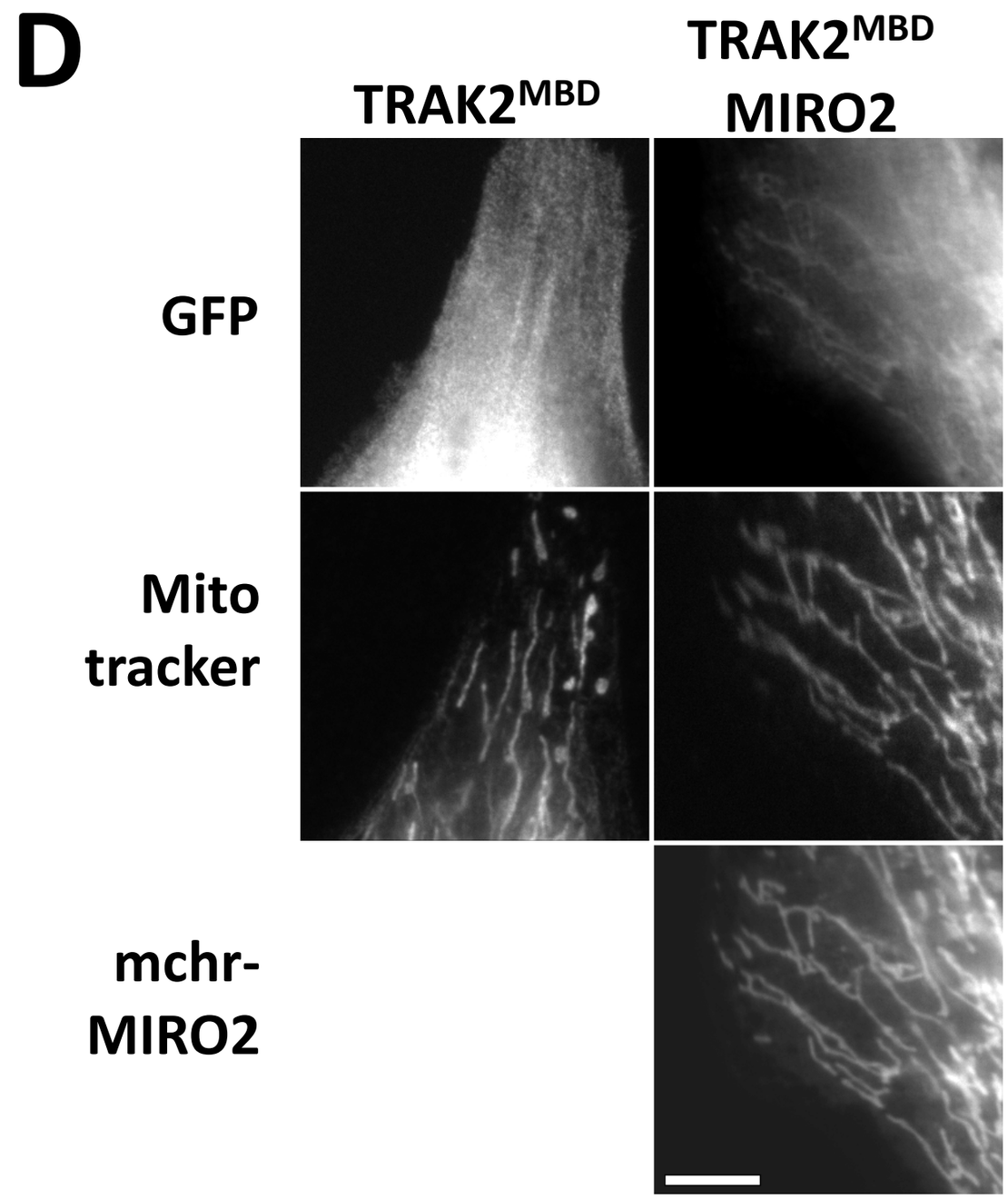
D
TRAK2MBD
TRAK2MBD MIRO2
GFP
Mito tracker
mchr-MIRO2

FIGURE 1

Figure 2: Ectopic mchr-MIRO2 expression modulated GFP-TRAK localization to mitochondria in MEF^{dko} cells. (A) Full length GFP-TRAK1 or GFP-TRAK2 constructs displayed enhanced fluorescence on mitochondria relative to cytoplasm, even in the absence of MIRO expression. Coexpression of mchr-MIRO2 increased the relative brightness of the GFP-TRAK2 fluorescence on mitochondria as compared to the cytoplasm (*$p<0.05$, t-test, n >= 28 cells per condition). (B) GFP-TRAK^{MBD} constructs only displayed enhanced mitochondria fluorescence when coexpressed with mchr-MIRO2 (*$p<0.05$, t-test, n >= 43 cells per condition). (C) Coexpression of mchr-MIRO2 decreased the percentage of cells showing primarily cytosolic localization of GFP-TRAK1, GFP-TRAK2, and GFP-TRAK2^{MBD} (*$p<0.05$, t-test, n >= 4 independent experiments per condition). Panel (D) shows representative images of the most common patterns observed in cells expressing GFP-TRAK2 and mchr-MIRO2 constructs. Scale bar, 10 μm.

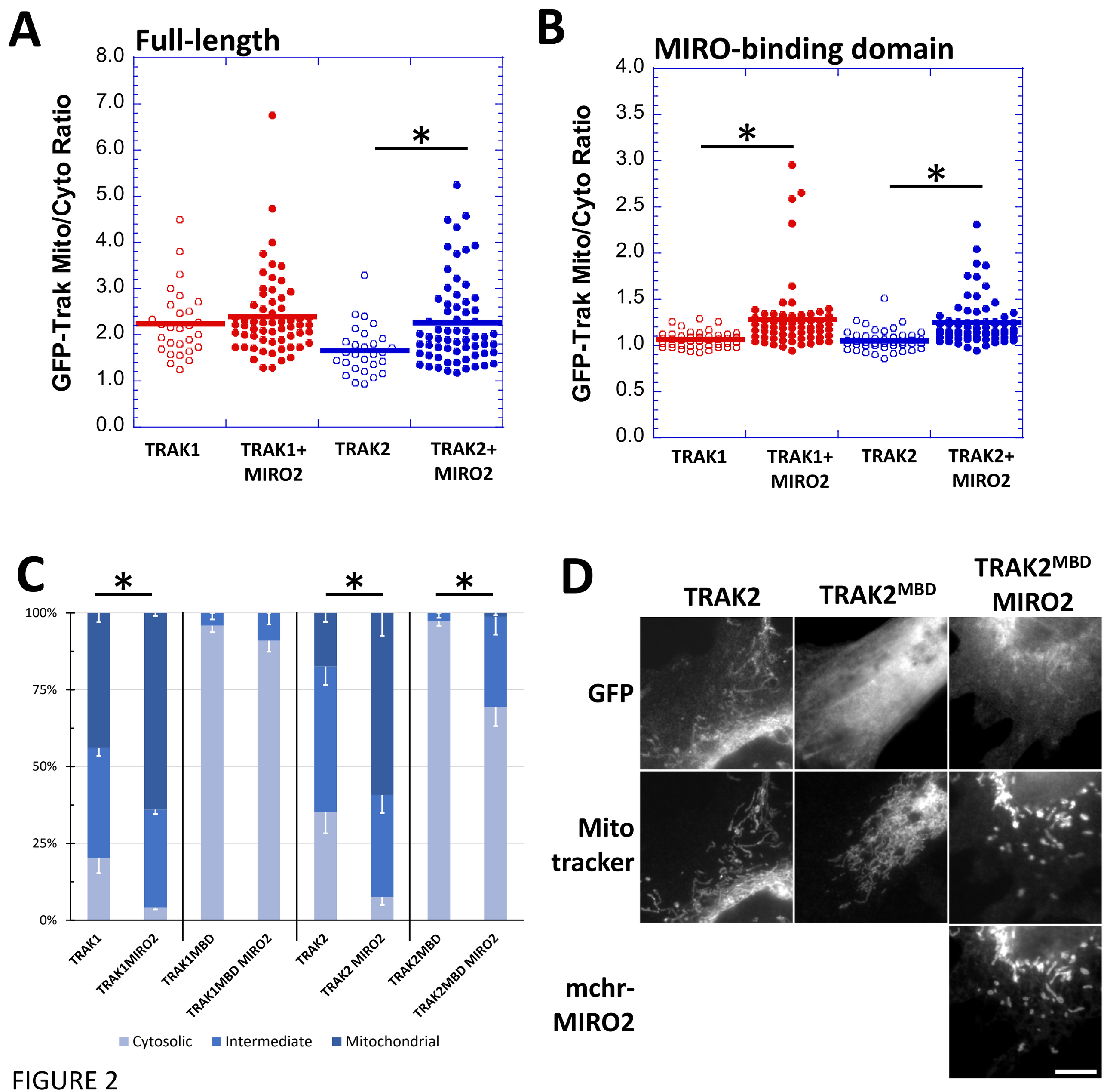
A
Full-length
GFP-Trak Mito/Cyto Ratio
8.0
7.0
6.0
5.0
4.0
3.0
2.0
1.0
0.0
*
TRAK1
TRAK1+ MIRO2
TRAK2
TRAK2+ MIRO2
B
MIRO-binding domain
GFP-Trak Mito/Cyto Ratio
4.0
3.5
3.0
2.5
2.0
1.5
1.0
0.5
0.0
*
*
TRAK1
TRAK1+ MIRO2
TRAK2
TRAK2+ MIRO2
C
*
*
*
100%
75%
50%
25%
0%
TRAK1
TRAK1MIRO2
TRAK1MBD
TRAK1MBD MIRO2
TRAK2
TRAK2 MIRO2
TRAK2MBD
TRAK2MBD MIRO2
Cytosolic
Intermediate
Mitochondrial
D
TRAK2
TRAK2MBD
TRAK2MBD MIRO2
GFP
Mito tracker
mchr-MIRO2

FIGURE 2

Figure 3: The MIRO-independent mitochondrial localization domain of TRAK is encoded by the amino acids c-terminal of the MIRO-binding domain. (A) GFP-TRAK1$^{C\text{-term}}$ expressed in MEF^{dko} cells displays brighter fluorescence in mitochondrial regions as compared to the cytosol regions, but to a lower degree than GFP-TRAK1. GFP-TRAK1$^{N\text{-term}}$ does not show brighter mitochondrial fluorescence (*$p<0.05$, Dunnett's test compared to full-length, $n \geq 28$ cells). (B) A similar pattern of results was obtained for GFP-TRAK2 constructs and truncations (*$p<0.05$, Dunnett's test compared to full-length, $n \geq 28$ cells). (C) The fraction of cells displaying primarily cytoplasmic fluorescence was smaller for full-length GFP-TRAK or the GFP-TRAK C-terminal constructs as compared to the GFP-TRAK N-terminal constructs (*$p>0.05$, Dunnett's test compared to N-terminal constructs, $n \geq 3$ independent experiments per condition). Panel (D) shows representative images of the most common patterns observed in cells expressing GFP-TRAK2 constructs. Scale bar, 10 μm.

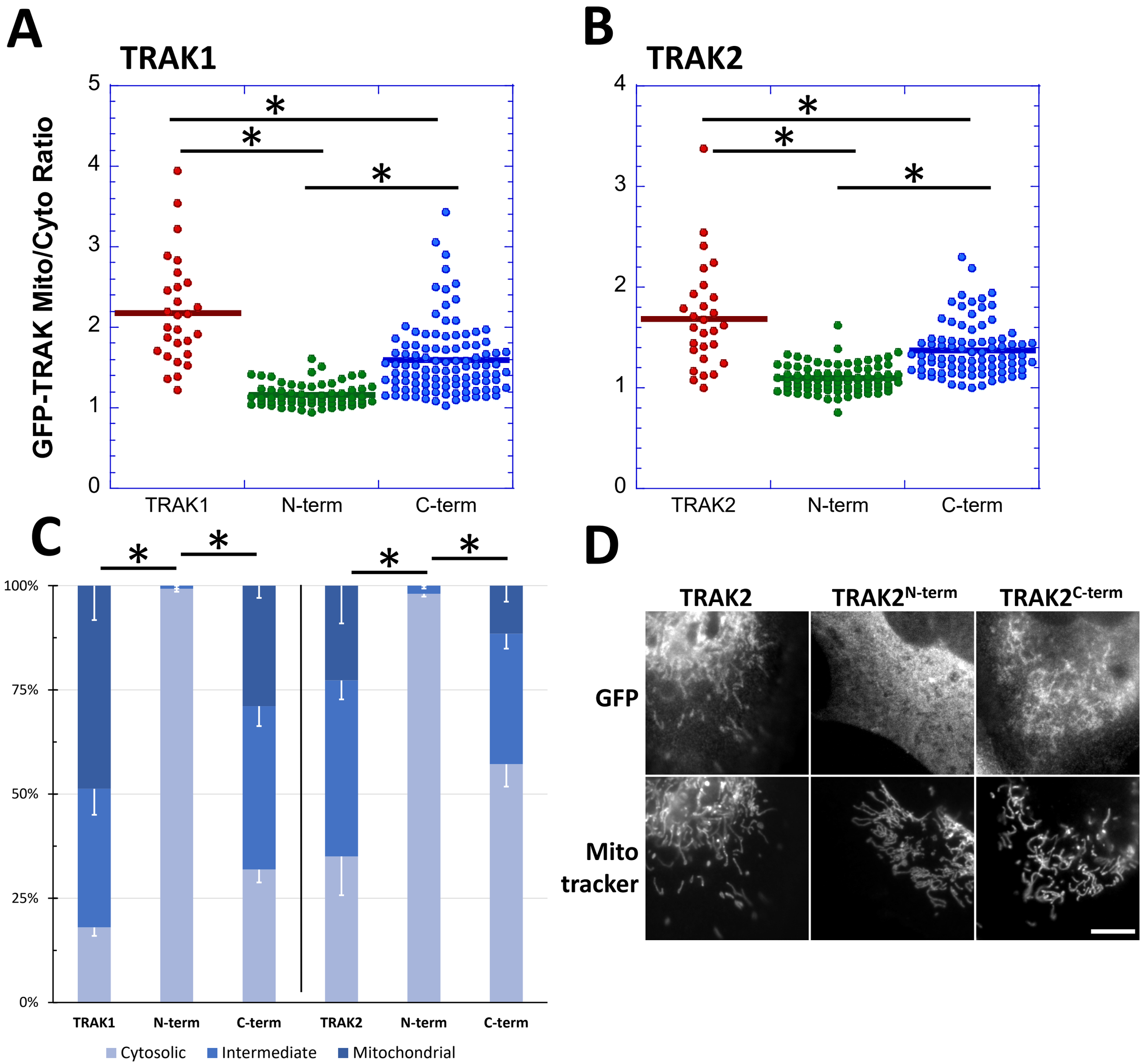
A
TRAK1
GFP-TRAK Mito/Cyto Ratio
5
4
3
2
1
0
*
*
*
TRAK1
N-term
C-term
B
TRAK2
4
3
2
1
0
*
*
*
TRAK2
N-term
C-term
C
100%
75%
50%
25%
0%
*
*
*
*
TRAK1
N-term
C-term
TRAK2
N-term
C-term
Cytosolic
Intermediate
Mitochondrial
D
TRAK2
TRAK2N-term
TRAK2C-term
GFP
Mito tracker

FIGURE 3

Figure 4: FRAP analysis reveals that GFP-TRAK^{MBD}/mchr-MIRO2 exchange kinetics are faster than MIRO-independent exchange kinetics for other GFP-TRAK constructs. GFP-tagged TRAK 1 (A) and TRAK2 (B) constructs were expressed in MEF^{dko} cells and analyzed for fluorescence recovery after photobleaching. Constructs capable of mitochondrial localization independent of MIRO expression & containing the C-terminal domain had significantly larger $t_{1/2}$, compared to GFP-TRAK^{MBD} expressed in MEFs coexpressing mchr-MIRO2. Points represent the mean ± standard error at each time point, and the curves are a double-exponential rise calculated from the averaged data, n>= 6. See Figure S1 for a summary of the analyses for all conditions.

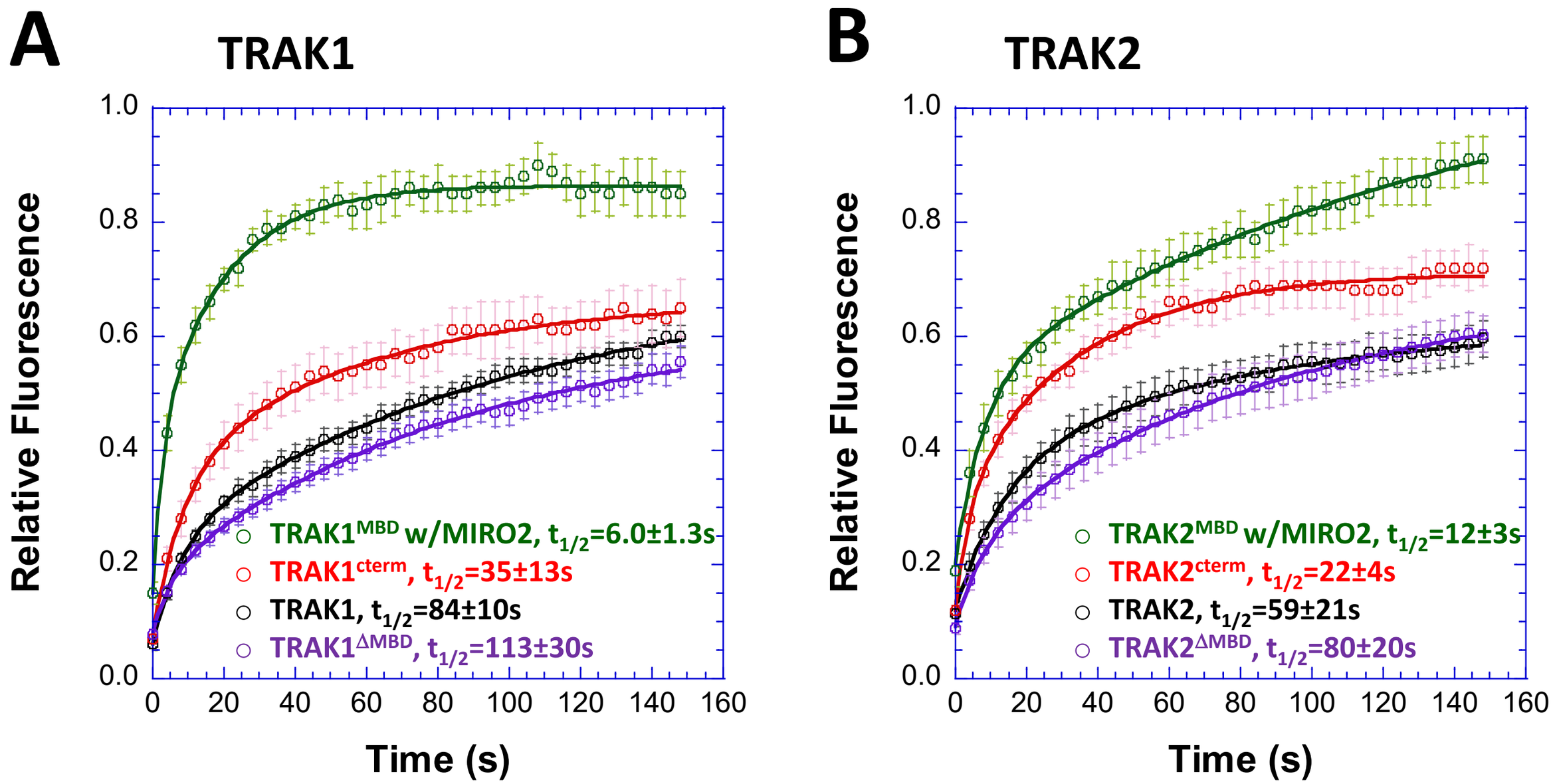
A
TRAK1
Relative Fluorescence
Time (s)
TRAK1MBD w/MIRO2, t1/2=6.0±1.3s
TRAK1cterm, t1/2=35±13s
TRAK1, t1/2=84±10s
TRAK1ΔMBD, t1/2=113±30s
B
TRAK2
Relative Fluorescence
Time (s)
TRAK2MBD w/MIRO2, t1/2=12±3s
TRAK2cterm, t1/2=22±4s
TRAK2, t1/2=59±21s
TRAK2ΔMBD, t1/2=80±20s

FIGURE 4

Figure 5: A kinetic model for MIRO interactions with molecular motor assemblies on the mitochondrial outer membrane. Our data indicate that TRAK is capable of MIRO-independent mitochondrial binding, and that MIRO-independent binding has slower turnover kinetics, indicating a tighter interaction than MIRO-dependent binding. Therefore, MIRO is likely serving to initially recruit TRAK and their associated MT motors to mitochondria, while tighter binding is mediated by the C-terminal domain. As a similar mechanism exists for MYO19, MIRO's function may be as an initial recruiter of a number of different proteins to the mitochondrial outer membrane, even if their mechanisms of MOM binding are different.

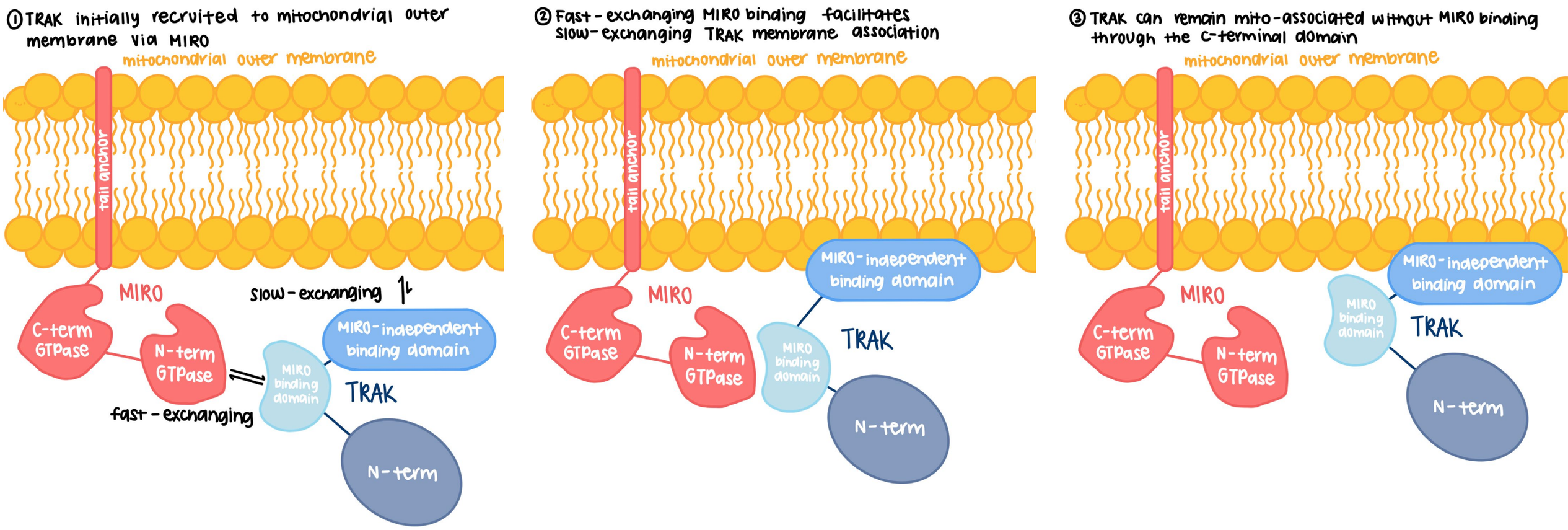
① TRAK initially recruited to mitochondrial outer membrane via MIRO
mitochondrial outer membrane
tail anchor
MIRO
C-term GTPase
N-term GTPase
slow-exchanging
fast-exchanging
MIRO binding domain
MIRO-independent binding domain
TRAK
N-term
② Fast-exchanging MIRO binding facilitates slow-exchanging TRAK membrane association
mitochondrial outer membrane
tail anchor
MIRO
C-term GTPase
N-term GTPase
MIRO binding domain
MIRO-independent binding domain
TRAK
N-term
③ TRAK can remain mito-associated without MIRO binding through the C-terminal domain
mitochondrial outer membrane
tail anchor
MIRO
C-term GTPase
N-term GTPase
MIRO binding domain
MIRO-independent binding domain
TRAK
N-term

FIGURE 5

Figure S1: Structural predictions of the minimal domain necessary for MIRO-independent mitochondrial association in the C-terminal regions of TRAK proteins. We used a combination of amphipathic helix prediction via MemBrain 3.1 and structural predictions from AlphaFold to attempt to identify the minimal number of residues encoding for the MIRO-independent mitochondrial association domain of mouse TRAK1 and TRAK2. Magenta letters represent hydrophobic amino acids, cyan highlighting corresponds to AlphaFold helix predictions, and underlines correspond to Membrain 3.1 amphipathic helix predictions (propensity score >0.3). When these truncations were expressed as GFP-tagged proteins in MEF^{dko} cells, neither $TRAK1^{min\text{-}C}$ nor $TRAK2^{min\text{-}C}$ localized to mitochondria--no matter whether the GFP-tag was N-terminal or C-terminal. For comparison, the MIRO-independent membrane association domain of human MYO19 is also shown, and $MYO19^{mem}$ does localize to mitochondria when expressed as a GFP-construct in MEF^{dko} cells.

TRAK1$^{min\text{-}C}$

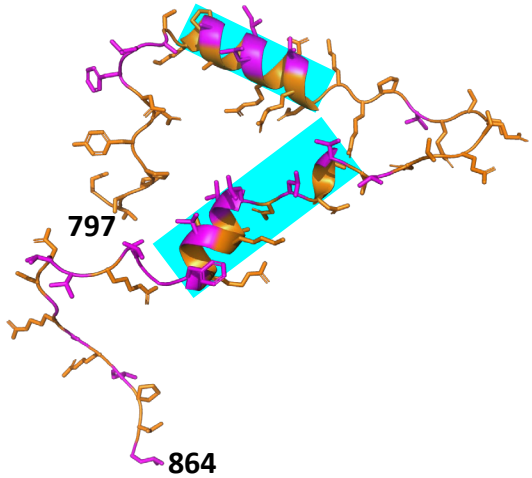

797- kcts ppynnflask passilrevr ekrpvrsses -830
831- qtdvsvsnln lvdkvrrfgv arvvnsgrar iptl -864

TRAK2$^{min\text{-}C}$

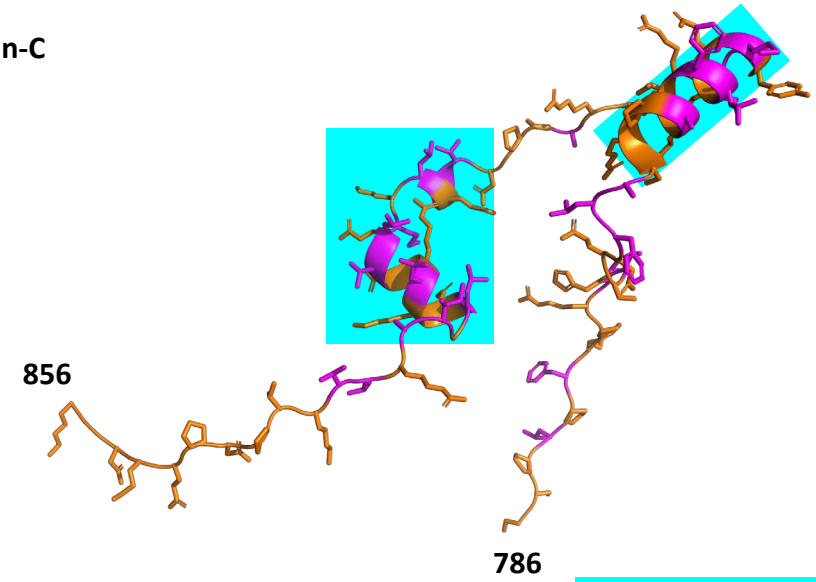

786- ssplp feprvhvsen flasrpaetf lqemyglrps -820
821- rappdvgqlk mnlvdrlkrl qiarvvktpd pqengk -856

MYO19^{mem}

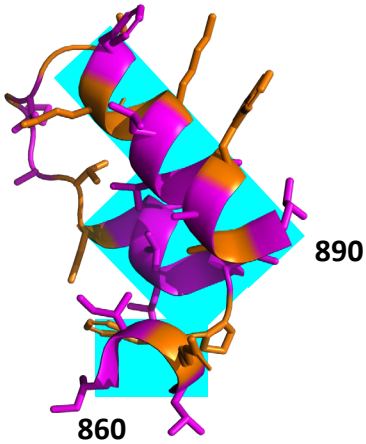

860- i irlwplglvl antamgvgsf qrklvvwacl -890

Fig S1

Figure S2: FRAP analysis reveals that GFP-MYO19 truncations construct exchange kinetics are slower than the kinetics for the corresponding GFP-TRAK constructs. (A) When expressed in MEF cells, GFP-MYO19^{MBD} in combination with mchr-MIRO2 tagged displayed slower exchange kinetics than what was observed for GFP-TRAK^{MBD} constructs coexpressed with mchr-MIRO2. Similarly, the TRAK constructs capable of MIRO-independent mitochondrial association (GFP-TRAK$^{C\text{-}term}$) displayed faster exchange kinetics than GFP-MYO19$^{860\text{-}890}$, which also displays MIRO-independent mitochondrial localization. Points represent the mean ± standard error at each time point, and the curves are a double-exponential rise calculated from the averaged data, n>= 6. (B) Rather than representing the fits calculated from the averaged data at each time point, the data in the table represent the descriptive statistics calculated from averaging the kinetic parameters from the number of individual fits represented by n.

A

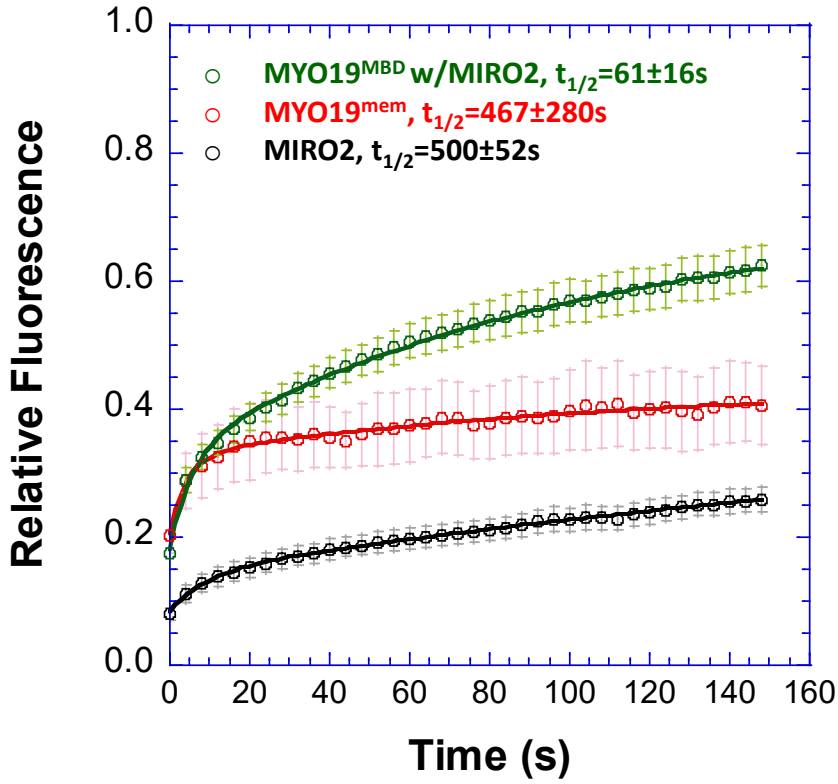

B

FRAP kinetic analysis of GFP constructs

	$t_{1/2}$ (s)	$Immobile_{600}$	n
TRAK1	89.8 ± 11.3	0.27±0.03	21
$TRAK1^{C\text{-}term}$	26.2± 3.8	0.32± 0.04	7
$TRAK1^{\Delta MBD}$	154±32*	0.28±0.04	13
$TRAK1^{MBD}$/mchr-Miro2	9.4±1.8*	0.17±0.03	8
TRAK2	98.1 ±26.2	0.25±0.05	14
$TRAK2^{C\text{-}term}$	26.5 ± 8.1*	0.28±0.04	10
$TRAK2^{\Delta MBD}$	97.3±16.5	0.22±0.04	12
$TRAK2^{MBD}$/mchr-Miro2	18.4 ± 5.7*	0.07 ±0.04*	6
$MYO19^{MBD}$/mchr-MIRO2	80.5±13.9	0.20±0.03	13
$MYO19^{mem}$	476±195	0.44±0.06	6
MIRO2	750±114	0.46±0.04	22

n represents the number of individual fits used to calculate mean ± standard error of the mean. *significantly different from corresponding full-length TRAK, $p < 0.05$, Dunnett's test.

Fig S2

Figure S3: Schematic diagrams of the fluorescent constructs used. GFP-tagged (A) Mouse TRAK1 and TRAK2 constructs were generated from the previously published constructs reported by Birsa et al. (Birsa et al., 2014). In addition to the reported truncations, the amino acid linker between the GFP domain and the TRAK protein was lengthened from SGLRSRAQAS to GEQKLRILQSTSGLRSRAQAS. (B) The mcherry- (Bocanegra et al., 2019) and GFP-tagged (Birsa et al., 2014) human MIRO2 constructs were previously reported. (C) The human GFP-MYO19^{MBD} (Bocanegra et al., 2019; Oeding et al., 2018) and GFP-MYO19^{mem} (Shneyer et al., 2016) constructs were also previously reported.

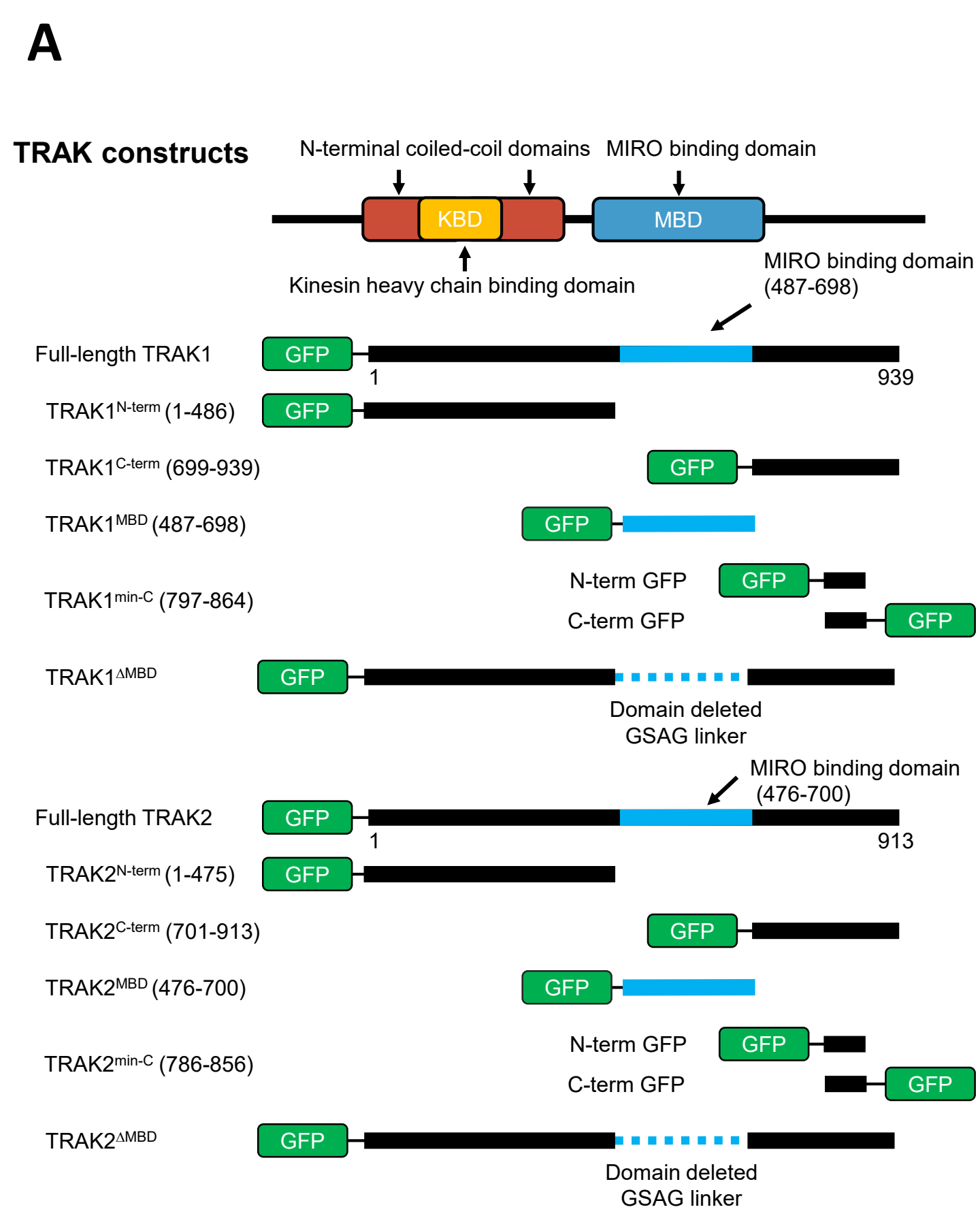
A
TRAK constructs
N-terminal coiled-coil domains
MIRO binding domain
KBD
MBD
Kinesin heavy chain binding domain
MIRO binding domain
(487-698)
Full-length TRAK1
GFP
1
939
TRAK1N-term (1-486)
TRAK1C-term (699-939)
TRAK1MBD (487-698)
TRAK1min-C (797-864)
N-term GFP
C-term GFP
TRAK1ΔMBD
Domain deleted
GSAG linker
MIRO binding domain
(476-700)
Full-length TRAK2
913
TRAK2N-term (1-475)
TRAK2C-term (701-913)
TRAK2MBD (476-700)
TRAK2min-C (786-856)
TRAK2ΔMBD

Fig S3A

B

MIRO2 constructs

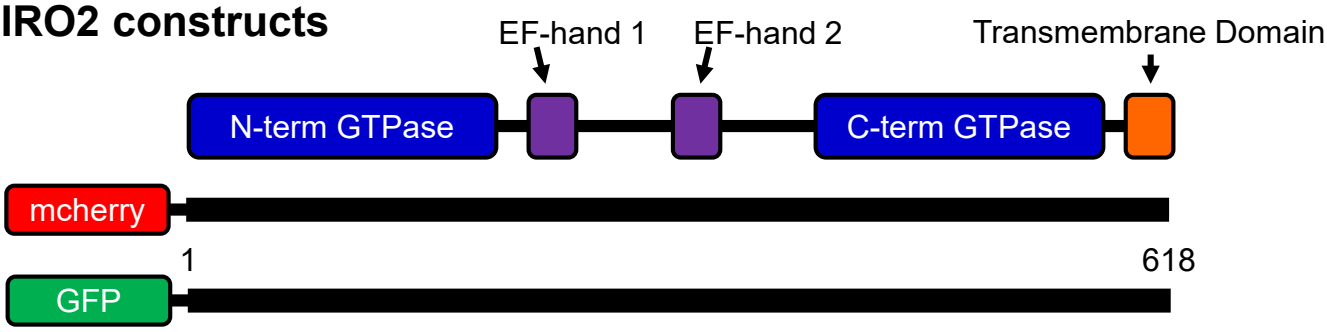

C

MYO19 tail constructs

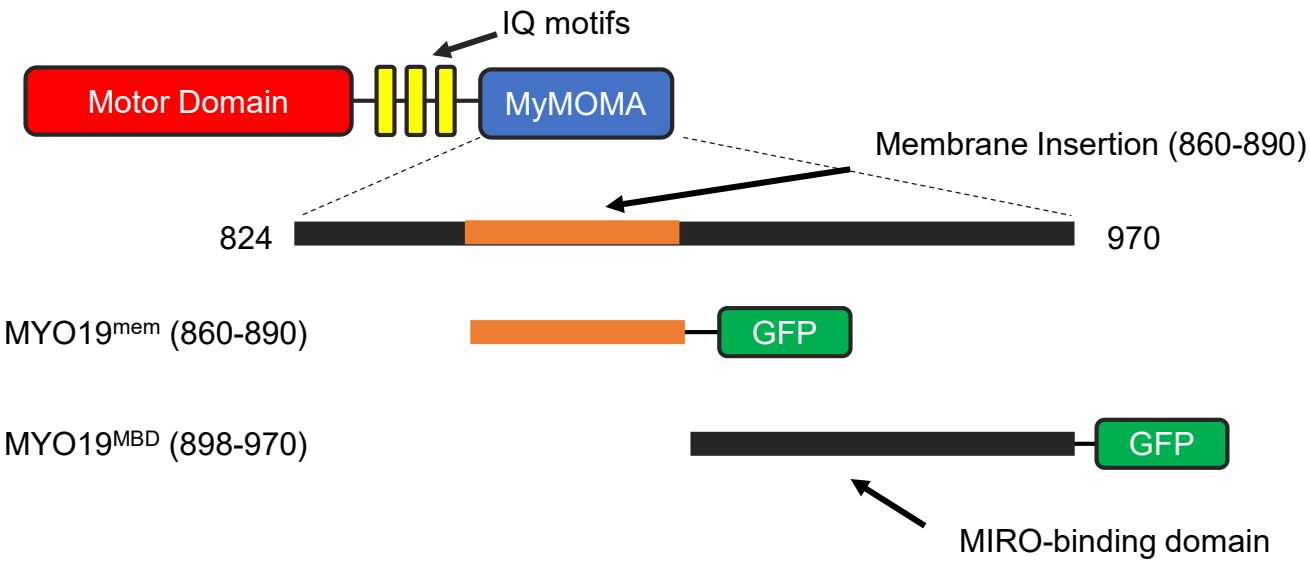

Fig S3B

Figure S4: Schematic diagrams of the quantitative imaging approaches used. (A) The ratio of mitochondrial fluorescence to cytoplasmic fluorescence was determining the mean fluorescence signal for the GFP channel in a ROI within the mitochondria and then dividing that value by the mean fluorescence for the GFP channel in an adjacent cytoplasmic region. (B) To determine the fraction of cells in a population displaying a particular phentotype (mitochondrial, cytosolic, or intermediate), the number of cells with a particular phenotype were divided by the total number of cells counted for that experimental condition. (C) Fluorescence recovery after photobleaching analysis involved photobleaching a region of interest and then collecting a time-lapse series following the photobleaching. The brightness value of the bleached ROI was normalized to the brightness value of that same ROI in the frame prior to bleaching, and corrected for photofading due to acquisition. The resulting data were then fit to a double-exponential rise, and the time to 50% of the initial brightness ($t_{1/2}$), determined from the double-exponential fit. Longer $t_{1/2}$ were interpreted as slower exchange of bleached fluors for unbleached fluors, indicating a stronger association of that particular fluor with its associated subcellular assembly.

A

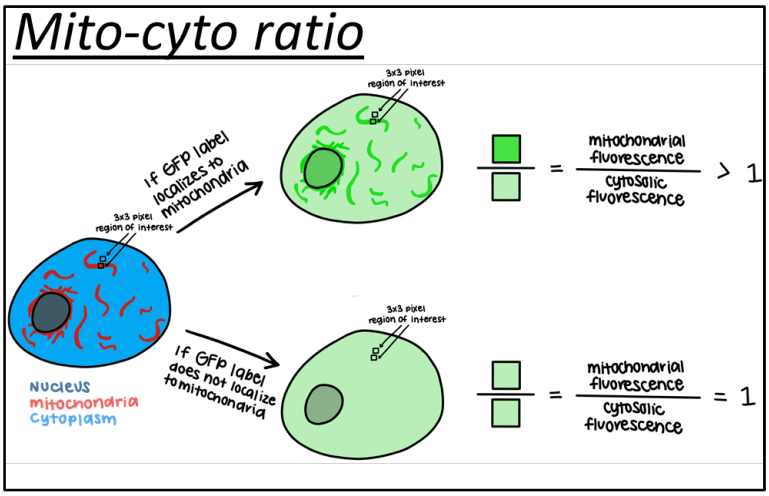
Mito-cyto ratio
3x3 pixel region of interest
If GFP label localizes to mitochondria
3x3 pixel region of interest
mitochondrial fluorescence
cytosolic fluorescence
> 1
Nucleus
mitochondria
cytoplasm
3x3 pixel region of interest
If GFP label does not localize to mitochondria
mitochondrial fluorescence
cytosolic fluorescence
= 1

B

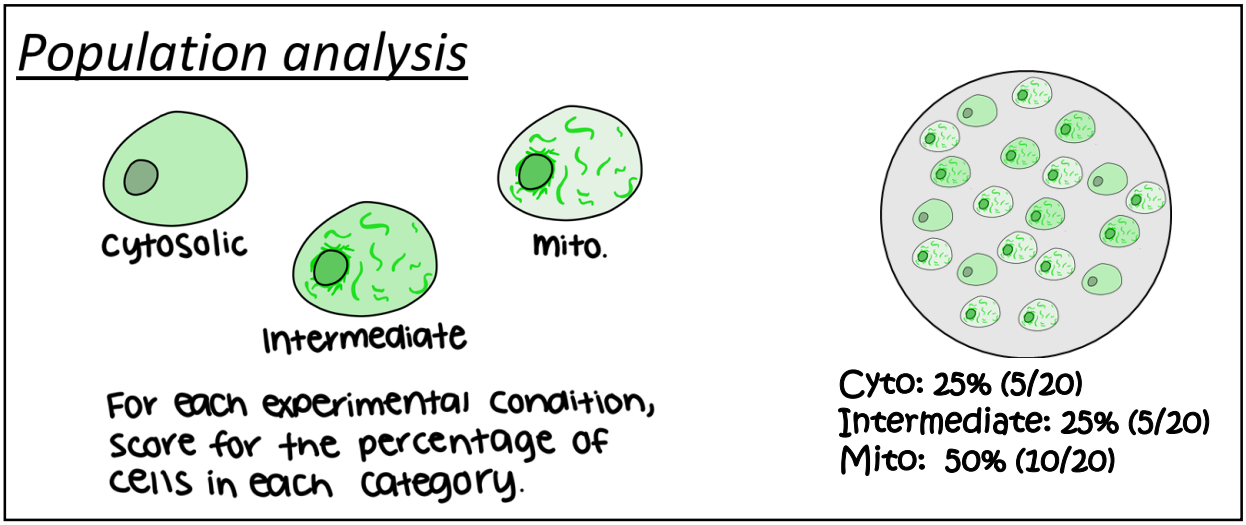
Population analysis
cytosolic
Intermediate
mito.
For each experimental condition, score for the percentage of cells in each category.
Cyto: 25% (5/20)
Intermediate: 25% (5/20)
Mito: 50% (10/20)

C

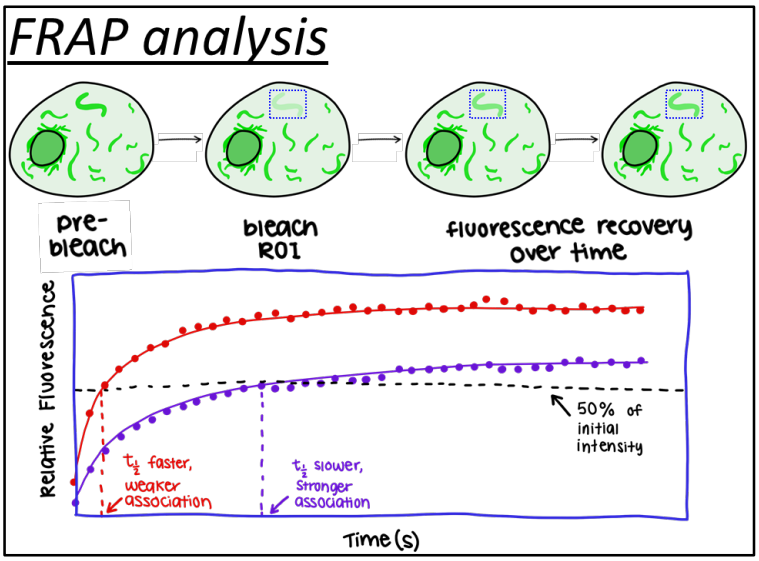
FRAP analysis
pre-bleach
bleach ROI
fluorescence recovery over time
Relative Fluorescence
50% of initial intensity
$t_{\frac{1}{2}}$ faster, weaker association
$t_{\frac{1}{2}}$ slower, stronger association
Time (s)

Fig S4

Materials and Methods

Construct generation

Human mchr-MIRO2 (Bocanegra et al., 2019) and GFP-MIRO2 (Birsa et al., 2014) were previously reported. Mouse GFP-TRAK constructs used in these studies were generated using previously reported GFP-TRAK plasmids (Lopez-Domenech et al., 2018) as a template, after the addition of an additional sequence of amino acids to the linker between the GFP and TRAK. Truncations were generated using PFU Ultra II PCR enzyme for megaprimer insertion PCR or deletion mutagenesis PCR, depending on the nucleotide changes required (Geiser et al., 2001), or ordered from Twist Bioscience. A schematic of the constructs used can be found in Figure S3.

Cell culture and transfection

HeLa cells (Scherer et al., 1953) and MIRO1/2 double-knockout mouse embryonic fibroblasts (MEF^{dko}) (Lopez-Domenech et al., 2018) were grown in DMEM high glucose (ThermoFisher) supplemented with 10% fetal bovine serum (Gemini Bio-products) 50 units/mL penicillin, and 50µg/mL streptomycin. Cells were maintained in a humidified incubator at 37˚C and 5%CO_2. Cells were passaged using 0.25% trypsin-EDTA. For imaging experiments, HeLa cells were grown on 22mm #1.5 glass coverslips. For live-cell experiments MEF^{dko} cells were grown on #1.5 coverslip glass-bottom 35mm dishes.

Cells were transfected with Lipofectamine 3000 (ThermoFisher) using a modified manufacturer′s protocol. For all experiments, 3µL of enhancer reagent, 1µg of GFP-tagged construct DNA were mixed with 0.5µg of mchr-tagged construct DNA and diluted in Optimem (ThermoFisher) without serum or antibiotics, in a final volume of 125µL per coverslip. In all experiments, 4µL of Lipofectamine was diluted into 125µL of Optimem without serum or

antibiotics and then mixed with the DNA dilution. Complexes were allowed to form for 5 minutes at room temperature. The entirety of the DNA/reagent mix was added drop-wise to a well of a 6-well plate or one glass-bottom dish. Cells were used for experimentation 14 to 30 hours after transfection.

Cell fixation and image acquisition

Transfected cells grown on coverslips were stained with 100nM Mitotracker DeepRed FM diluted in growth media for 10 minutes, and then washed in growth media for 10 minutes. Cells were then fixed in PBS with 4% paraformaldehyde 37˚C. After permeabilization in PBS with 0.5% TritonX-100 for 5 minutes, cells were stained in PBS with 3.3 nM ALEXA plus 405-phallodin for 20 minutes to label the actin cytoskeleton. Coverslips were washed in PBS four times for five minutes and mounted on slides using PBS in 80% glycerol and 0.5% N-propyl gallate. Coverslips were sealed onto slides with Sally Hansen Hard as Nails clear nail polish.

Images were acquired using an Olympus IX-83 microscope and a PLAN APON 60x/1.42NA DIC objective. Cells were illuminated using an EXFO mixed gas light source, Sedat Quad filters (Chroma), and Sutter filter wheels & shutters. Images were acquired using a Hamamatsu ORCA-Flash 4.0 V2 sCMOS camera, and Metamorph imaging software to control the system components. In all instances, exposure times maintained constant across experimental data sets.

Mito/Cyto Ratio calculation

The ratio of mitochondria localized fluorescence to cytosol localized fluorescence (mito/cyto ratio, MCR) was calculated by measuring the mean gray value of mitochondria and

cytosol with 3×3 pixel boxes using FIJI software. The ratio was calculated for five separate regions within one cell and then averaged across the cell.

The assumption of the MCR is that GFP-TRAK fluorescence will evenly disperse throughout the entire cell unless TRAK is specifically targeted to a cellular location, such as the mitochondria. "Mitochondrial regions" of cells were identified by using the Mitotracker channel. Mitochondrial boxes were placed where mitochondria were visible. Boxes were placed for "cytosolic regions" adjacent to mitochondrial boxes in areas of low fluorescence where no mitochondria were present. Measurements were not obtained from the Mitotracker channel. Instead, mito and cyto boxes placed in the Mitotracker channel were applied to corresponding images from the "GFP-TRAK" channel. The fluorescence of the mitochondria relative to the fluorescence of the cytosol in the GFP-TRAK channel thus indicated the relative concentration of TRAK proteins in mitochondrial regions compared to the cytoplasm. An MCR that has a value greater than 1 indicates that mitochondria-associated GFP-TRAK fluorescence was greater than cytosolic GFP-TRAK fluorescence. An MCR equal to 1 indicates that TRAK was not localizing differently between the mitochondria and the cytoplasm (see Figure S4A for a schematic).

Population analysis of phenotypes

Phenotypic variability exists in any population of cells or organisms. Cells were visually scored to identify the prevalence of strongly localized GFP-TRAK across the population of cells by assigning cells to one of three categories: cytosolic, mitochondrial, or intermediate localization (Bocanegra et al., 2019). Cells characterized as "cytosolic" cells showed no distinct GFP-TRAK fluorescence in mitochondrial regions, while cells characterized as "mitochondrial"

displayed strong fluorescence in mitochondrial regions with little fluorescence in cytosolic regions. “Intermediate” cells exhibited strong fluorescence in mitochondrial regions in conjunction with some fluorescence in cytosolic regions. During population scoring, the data collector was blinded to the identity of the samples. The fraction of cells exhibiting each TRAK localization phenotype was calculated by manually scoring 60-100 cells per coverslip. The percentage of cells of each phenotype was calculated by dividing the number of cells of a specific phenotype by the total number of cells counted for the coverslip (see Figure 4B for a schematic).

Fluorescence recovery after photobleaching (FRAP) analysis

Cells were grown on coverslip-glass-bottom dishes prior to transfection as previously described. For live-cell imaging, growth media was exchanged for imaging media (Optimem without phenol red containing 50 units/mL penicillin, and 50µg/mL streptomycin), and cells were maintained in a humidified environment at 37°C and 5% CO_2 using a stage-top OKO-labs incubation chamber. Images were collected on an Olympus FV1200 laser scanning confocal microscope outfitted with a PLAN APON 60x/1.4NA objective at a frame-rate of 1 frame every 4 seconds. After the first 15 frames, regions of interest were illuminated for photobleaching at high laser power for 1 second. FIJI was used to identify regions of interest and calculate average fluorescence intensity for each time point. Relative fluorescence at each time point was measured by determining the fluorescence intensity relative to the frame prior to photobleaching (t = 0s). Data were corrected for photofading due to imaging (Applewhite et al., 2007) and averaged together. The mean gray value relative to t = 0 was plotted over time and fit to the function $y = a*(1 - e^{-bt}) + c*(1 - e^{-dt}) + e$. The half-life ($t_{1/2}$) was calculated using from the

exponential rise function by calculating the value of t when y = 0.5 (see Figure S4C for a schematic). Immobile fraction was calculated by determining the asymptote being approached at time = 600s. Regions of interest chosen for analysis were of sections of a reticular mitochondrial network, rather than of isolated mitochondrial particles.

Quantification, analysis, and statistics

Metamorph (Universal Imaging) and FIJI were used for image analysis. Data points are expressed as means ± standard error of the mean. Data were compared by Student's t-test or Dunnett's analysis using Kaleidagraph. Exponential fits for FRAP analysis were performed using Kaleidagraph. Parameters calculated from exponential fits in the data table are expressed as mean ± the SEM calculated across individual samples. Parameters shown on the graphs are calculated as mean ± the SEM -adjusted fit (Singh et al., 2016), by generating curve fits of the mean + SEM and mean − SEM, and reporting the error as the difference between the value calculated from the mean fit and the value calculated from the SEM-adjusted fit. All images were prepared for publication using FIJI, Metamorph, Photoshop, or some combination of these software packages.

References

Applewhite, D.A., Barzik, M., Kojima, S., Svitkina, T.M., Gertler, F.B., and Borisy, G.G. (2007). Ena/VASP proteins have an anti-capping independent function in filopodia formation. Mol Biol Cell *18*, 2579-2591.

Beck, M., Brickley, K., Wilkinson, H.L., Sharma, S., Smith, M., Chazot, P.L., Pollard, S., and Stephenson, F.A. (2002). Identification, molecular cloning, and characterization of a novel GABAA receptor-associated protein, GRIF-1. J Biol Chem *277*, 30079-30090.

Birsa, N., Norkett, R., Wauer, T., Mevissen, T.E., Wu, H.C., Foltynie, T., Bhatia, K., Hirst, W.D., Komander, D., Plun-Favreau, H.*, et al.* (2014). Lysine 27 ubiquitination of the mitochondrial transport protein Miro is dependent on serine 65 of the Parkin ubiquitin ligase. J Biol Chem *289*, 14569-14582.

Bocanegra, J.L., Fujita, B.M., Melton, N.R., Cowan, J.M., Schinski, E.L., Tamir, T.Y., Major, M.B., and Quintero, O.A. (2019). The MyMOMA domain of MYO19 encodes for distinct Miro-dependent and Miro-independent mechanisms of interaction with mitochondrial membranes. Cytoskeleton (Hoboken).

DiMauro, S. (1999). Mitochondrial encephalomyopathies: back to Mendelian genetics. Ann Neurol *45*, 693-694.

Feng, S.H., Xia, C.Q., Zhang, P.D., and Shen, H.B. (2022). Ab-Initio Membrane Protein Amphipathic Helix Structure Prediction Using Deep Neural Networks. IEEE/ACM Trans Comput Biol Bioinform *19*, 795-805.

Fenton, A.R., Jongens, T.A., and Holzbaur, E.L.F. (2020). Mitochondrial dynamics: Shaping and remodeling an organelle network. Curr Opin Cell Biol *68*, 28-36.

Fenton, A.R., Jongens, T.A., and Holzbaur, E.L.F. (2021). Mitochondrial adaptor TRAK2 activates and functionally links opposing kinesin and dynein motors. Nature communications *12*, 4578.

Fransson, A., Ruusala, A., and Aspenstrom, P. (2003). Atypical Rho GTPases have roles in mitochondrial homeostasis and apoptosis. J Biol Chem *278*, 6495-6502.

Fransson, S., Ruusala, A., and Aspenstrom, P. (2006). The atypical Rho GTPases Miro-1 and Miro-2 have essential roles in mitochondrial trafficking. Biochem Biophys Res Commun *344*, 500-510.

Geiser, M., Cebe, R., Drewello, D., and Schmitz, R. (2001). Integration of PCR fragments at any specific site within cloning vectors without the use of restriction enzymes and DNA ligase. BioTechniques *31*, 88-90, 92.

Glater, E.E., Megeath, L.J., Stowers, R.S., and Schwarz, T.L. (2006). Axonal transport of mitochondria requires milton to recruit kinesin heavy chain and is light chain independent. J Cell Biol *173*, 545-557.

Guo, X., Macleod, G.T., Wellington, A., Hu, F., Panchumarthi, S., Schoenfield, M., Marin, L., Charlton, M.P., Atwood, H.L., and Zinsmaier, K.E. (2005). The GTPase dMiro is required for axonal transport of mitochondria to Drosophila synapses. Neuron *47*, 379-393.

Howard, J. (2001). Mechanics of Motor Proteins and the Cytoskeleton (Sunderland: Sinauer Associates, Inc.).

Iyer, S.P., Akimoto, Y., and Hart, G.W. (2003). Identification and cloning of a novel family of coiled-coil domain proteins that interact with O-GlcNAc transferase. J Biol Chem *278*, 5399-5409.

Jumper, J., Evans, R., Pritzel, A., Green, T., Figurnov, M., Ronneberger, O., Tunyasuvunakool, K., Bates, R., Zidek, A., Potapenko, A.*, et al.* (2021). Highly accurate protein structure prediction with AlphaFold. Nature *596*, 583-589.

Kruppa, A.J., and Buss, F. (2021). Motor proteins at the mitochondria-cytoskeleton interface. J Cell Sci *134*.

Lopez-Domenech, G., Covill-Cooke, C., Ivankovic, D., Halff, E.F., Sheehan, D.F., Norkett, R., Birsa, N., and Kittler, J.T. (2018). Miro proteins coordinate microtubule- and actin-dependent mitochondrial transport and distribution. EMBO J *37*, 321-336.

MacAskill, A.F., Brickley, K., Stephenson, F.A., and Kittler, J.T. (2009). GTPase dependent recruitment of Grif-1 by Miro1 regulates mitochondrial trafficking in hippocampal neurons. Molecular and cellular neurosciences *40*, 301-312.

Oeding, S.J., Majstrowicz, K., Hu, X.P., Schwarz, V., Freitag, A., Honnert, U., Nikolaus, P., and Bahler, M. (2018). Identification of Miro as a mitochondrial receptor for myosin XIX. J Cell Sci.

Oughtred, R., Rust, J., Chang, C., Breitkreutz, B.J., Stark, C., Willems, A., Boucher, L., Leung, G., Kolas, N., Zhang, F.*, et al.* (2021). The BioGRID database: A comprehensive biomedical resource of curated protein, genetic, and chemical interactions. Protein Sci *30*, 187-200.

Panchal, K., and Tiwari, A.K. (2021). Miro (Mitochondrial Rho GTPase), a key player of mitochondrial axonal transport and mitochondrial dynamics in neurodegenerative diseases. Mitochondrion *56*, 118-135.

Pilling, A.D., Horiuchi, D., Lively, C.M., and Saxton, W.M. (2006). Kinesin-1 and Dynein are the primary motors for fast transport of mitochondria in Drosophila motor axons. Mol Biol Cell *17*, 2057-2068.

Pollard, T.D., and De La Cruz, E.M. (2013). Take advantage of time in your experiments: a guide to simple, informative kinetics assays. Mol Biol Cell *24*, 1103-1110.

Quintero, O.A., DiVito, M.M., Adikes, R.C., Kortan, M.B., Case, L.B., Lier, A.J., Panaretos, N.S., Slater, S.Q., Rengarajan, M., Feliu, M.*, et al.* (2009). Human Myo19 is a novel myosin that associates with mitochondria. Curr Biol *19*, 2008-2013.

Scherer, W.F., Syverton, J.T., and Gey, G.O. (1953). Studies on the propagation in vitro of poliomyelitis viruses. IV. Viral multiplication in a stable strain of human malignant epithelial cells (strain HeLa) derived from an epidermoid carcinoma of the cervix. J Exp Med *97*, 695-710.

Shneyer, B.I., Usaj, M., and Henn, A. (2016). Myo19 is an outer mitochondrial membrane motor and effector of starvation-induced filopodia. J Cell Sci *129*, 543-556.

Singh, P.P., Hawthorne, J.L., and Quintero, O.A. (2016). Permeabilization Activated Reduction in Fluorescence (PARF): a novel method to measure kinetics of protein interactions with intracellular structures. Cytoskeleton *73*, 271-285.

Smith, M.J., Pozo, K., Brickley, K., and Stephenson, F.A. (2006). Mapping the GRIF-1 binding domain of the kinesin, KIF5C, substantiates a role for GRIF-1 as an adaptor protein in the anterograde trafficking of cargoes. J Biol Chem *281*, 27216-27228.

Stowers, R.S., Megeath, L.J., Gorska-Andrzejak, J., Meinertzhagen, I.A., and Schwarz, T.L. (2002). Axonal transport of mitochondria to synapses depends on milton, a novel Drosophila protein. Neuron *36*, 1063-1077.

van Spronsen, M., Mikhaylova, M., Lipka, J., Schlager, M.A., van den Heuvel, D.J., Kuijpers, M., Wulf, P.S., Keijzer, N., Demmers, J., Kapitein, L.C.*, et al.* (2013). TRAK/Milton motor-adaptor proteins steer mitochondrial trafficking to axons and dendrites. Neuron *77*, 485-502.

Varadi, M., Anyango, S., Deshpande, M., Nair, S., Natassia, C., Yordanova, G., Yuan, D., Stroe, O., Wood, G., Laydon, A.*, et al.* (2022). AlphaFold Protein Structure Database: massively expanding the structural coverage of protein-sequence space with high-accuracy models. Nucleic Acids Res *50*, D439-D444.

Wait, E.C., Reiche, M.A., and Chew, T.L. (2020). Hypothesis-driven quantitative fluorescence microscopy - the importance of reverse-thinking in experimental design. J Cell Sci *133*.

Wallace, D.C. (1999). Mitochondrial diseases in man and mouse. Science *283*, 1482-1488.

Wang, C., and Youle, R.J. (2009). The role of mitochondria in apoptosis*. Annu Rev Genet *43*, 95-118.

Wang, X., and Schwarz, T.L. (2009). The mechanism of Ca2+ -dependent regulation of kinesin-mediated mitochondrial motility. Cell *136*, 163-174.